0D Model of Magnetized Hydrogen Helium Wall Conditioning Plasmas

T. Wauters[1], A. Lyssoivan[2], D. Douai[1], O. Marchuk[3], D. Wünderlich[4], R. Koch[2], G. Sergienko[3], G. Van Oost[5] and M. Van Schoor[2]

[1] CEA, IRFM, Association Euratom-CEA, 13108 St Paul lez Durance, France
[2] LPP-ERM/KMS, Association Euratom-Belgian State, 1000 Brussels, Belgium
[3] IEF-Plasmaphysik FZ Jülich, Euratom Association, 52425 Jülich, Germany
[4] Max-Planck Institut für Plasmaphysik, Euratom Association, 85748 Garching, Germany
[5] Ghent University, Department of Applied Physics, 9000 Ghent, Belgium.

E-mail: tom.wauters@cea.fr

Abstract. In this paper the 0D description of magnetized toroidal hydrogen-helium RF discharges is presented. The model has been developed to obtain insight on ICRF plasma parameters, particle fluxes to the walls and the main collisional processes, which is especially relevant for the comprehension of RF wall conditioning discharges. The 0D plasma description is based on the energy and particle balance equations for 9 principal species: H, H^+, H_2, H_2^+, H_3^+, He, He^+, He^{2+} and e^-. It takes into account (1) elementary atomic and molecular collision processes, such as excitation/radiation, ionization, dissociation, recombination, charge exchange, etc... and elastic collisions, (2) particle losses due to the finite dimensions of the plasma volume and confinement properties of the magnetic configuration, and particle recycling, (3) active pumping and gas injection, (4) RF heating of electrons (and protons) and (5) a qualitative description of plasma impurities. The model reproduces experimental plasma density dependencies on discharge pressure and coupled RF power, both for hydrogen RF discharges ($n_e \approx 1 - 5 \cdot 10^{10}\,\mathrm{cm}^{-3}$) as for helium discharges ($n_e \approx 1 - 5 \cdot 10^{11}\,\mathrm{cm}^{-3}$). The modeled wall fluxes of hydrogen discharges are in the range of what is estimated experimentally: $\sim 10^{19} - 10^{20}\,/\mathrm{m}^2\mathrm{s}$ for H-atoms, and $\sim 10^{17} - 10^{18}\,/\mathrm{m}^2\mathrm{s}$ for H^+-ions. It is found that experimentally evidenced impurity concentrations have an important impact on the plasma parameters, and that wall desorbed particles contribute largely to the total wall flux.

PACS numbers: 52.50.Qt, 52.55.Dy, 52.65.-y, 52.80.Pi

1. Introduction

In this paper the 0D description of a hydrogen-helium plasma implemented in TOMATOR-0D (0D Transport Oriented model for MAgnetized TOroidal Rf discharges) is outlined. The model has been developed to describe the evolution of ICRF plasmas from discharge initiation to the (quasi) steady state plasma stage. The radio-frequency (RF) plasma production technique in the Ion Cyclotron Range of Frequency (ICRF) attracts growing attention among fusion experts because of its high potential for solving several basic problems of reactor oriented superconducting fusion machines. The ICRF plasma parameters will differ according to the application:

- ICRF wall conditioning in tokamaks [1, 2, 3] and stellarators [4]: In wall conditioning applications one intends to create a high and homogeneous flux of particles to the walls to provoke chemical and physical processes on the plasma facing components. Wall conditioning objectives are facilitating tokamak plasma start-up and improving its performance by e.g. reducing the amount of impurities on the wall or lowering the recycling of particles [5], and in future machines wall conditioning can be used to mitigate the tritium inventory build-up [6]. The envisaged plasma parameters for ICRF wall conditioning are low plasma density $n_e = 10^{10} - 10^{12}\,\mathrm{cm}^{-3}$ and low electron temperature $T_e = 1 - 5\,\mathrm{eV}$. These temperatures cover a range wherein a hydrogen or helium plasma can have an ionization degree of a few percent up to full ionization. The modeling efforts on hydrogen-helium RF discharges are mainly motivated by the urgent need to consolidate the Ion Cyclotron Wall Conditioning (ICWC) technique, which is presently the main technique envisioned for the conditioning of the ITER first wall in the presence of the toroidal magnetic field [7], and for which helium and hydrogen are the most common discharge gases.
- ICRF assisted tokamak start-up [8]: In ICRF assisted tokamak start-up the aim is to produce a dense target plasma ($n_e = 10^{12}\,\mathrm{cm}^{-3}$) before the start of the ohmic discharge, to reduce the inductive toroidal electric field requirements and the magnetic flux consumption in the primary coils during the breakdown phase.
- Target plasma production ($n_{e0} = 10^{13}\,\mathrm{cm}^{-3}$) in stellarators [9]: In a stellarator, where ohmic breakdown is not possible, plasma production in the ICRF band is a possible way to build up a dense target plasma [10].

The 0D model allows to study ICRF plasma build-up for the above applications in the mentioned typical density ranges, up to $n_e = 10^{13}\,\mathrm{cm}^{-3}$, and temperature range of $T_e = 1 - 10^3\,\mathrm{eV}$ (limited by reaction rate data). It gives insight on ICRF plasma parameters, particle fluxes to the walls and main collisional processes, the latter being the fundamental mechanism for the build-up of a plasma. This is of particular importance since most standard tokamak plasma diagnostics are not adapted to accurately diagnose these typical low temperature and low density plasmas. Together with experimental data, the model can thus be used to obtain better understanding of

the physics behind ICRF plasma production.

This paper is divided into two parts. A first part (section 2) is devoted to the description of the implemented model equations. In section 2.2 the included elementary inelastic and elastic collisions are listed, in section 2.3 the particle confinement properties and edge conditions (particle recycling) are outlined, in section 2.4 the implementation of the discharge control parameters (e.g. active gas throughput and coupled RF power) into the balance equations is given and finally in section 2.5 the balance equation adaptations to include impurities are introduced. Throughout these sections comments will be given on the effect of the different processes on the modeling results. In the second part of this paper (section 3), an overview of modeling results is given including a comparison with experimental data. To check the balance equations, in section 3.1 the plasma parameters are analyzed as a function of electron temperature and compared to literature, and in section 3.2 the plasma parameters are modeled as a function of discharge pressure and coupled power for hydrogen, helium and hydrogen/helium discharges, and compared to experimental data of TEXTOR and TORE SUPRA. Also temporal dependencies have been successfully modeled and are presented in [11].

2. Model description

2.1. Balance equations

To describe numerically in a 0D approach the evolution of ICRF plasma parameters in tokamaks and stellarators, a set of transport equations [12, 13, 14, 15] was adopted. The equations are derived from the standard continuity and heat balance equations given by Braginskii [16], where all particle species are assumed to have a Maxwellian energy distribution. In the present model the transport equations are updated to include molecular hydrogen and helium, which is especially of importance for wall conditioning plasmas. The 0D plasma description is based on the energy and particle balance equations for 9 species: H, H^+, H_2, H_2^+, H_3^+, He, He^+, He^{2+} and e^-. It takes into account (1) elementary atomic and molecular collision processes, such as excitation/radiation, ionization, dissociation, recombination, charge exchange, etc... and elastic collisions, (2) particle losses due to the finite dimensions of the plasma volume and confinement properties of the magnetic configuration, and particle recycling, (3) active pumping and gas injection, (4) RF heating of electrons (and protons) and (5) a qualitative description of plasma impurities, as shown in eq. (1) and (2),

$$\frac{\mathrm{d}n_p}{\mathrm{d}t} = \sum_{j<k}\sum_i \epsilon^i_{jkp} k^i_{jk} n_j n_k - \frac{n_p}{\tau_p} + Q_{\mathrm{S},p} - Q_{\mathrm{L},p} \tag{1}$$

$$\begin{aligned}\frac{3}{2}\frac{\mathrm{d}\widetilde{n_pT_p}}{\mathrm{d}t} = \dot{E}_p &= \sum_{j<k}\sum_i \epsilon^i_{jkp} E^i_{jkp} k^i_{jk} n_j n_k + \sum_j E_{jp} k^{\mathrm{el}}_j n_j n_p \\ &\quad - \frac{3}{2}\frac{\widetilde{n_pT_p}}{\tau_{E,p}} + Q_{\mathrm{S}E,p} - Q_{\mathrm{L}E,p} + P_{\mathrm{RF},p}\end{aligned} \tag{2}$$

where n_p and T_p are the population density and Maxwellian temperature, k^i_{jk} is the reaction rate for reaction i between particles of population j and k, E^i_{jkp} the corresponding energy change for the involved populations and ϵ^i_{jkp} accounts the number of lost or gained particles for each population, τ_p and $\tau_{E,p}$ are the particle and energy confinement time, $Q_{\mathrm{S},p}$ and $Q_{\mathrm{L},p}$ are external particle sources and losses with corresponding energy sources $Q_{\mathrm{SE},p}$ and losses $Q_{\mathrm{LE},p}$, and finally E_{jp} is the energy transfer from population j to p due to elastic collisions, with k^{el}_j the elastic collision reaction rate. In the following sections the equation elements are thoroughly discussed.

2.2. Elementary processes in hydrogen-helium plasmas

In this section all the included atomic and molecular reactions that are relevant for the model are described. The model does not treat excited states as separate species. Since cross sections are mostly dependent on the excited state of the involved particle, radiative-collisional models (RC) [17, 18] are applied where possible to obtain effective rate coefficients.

2.2.1. Inelastic electron impact reactions

- Electron collisions with H, H^+ (Table 1, 1-3): The effective reaction rates are calculated taking into account excited states of the hydrogen atom up to $n = 5$, where n is the principal quantum number. The excitation rate coefficients are based on K-matrix calculations [19] and all the values used were compared with recommended close-coupling calculations [20]. The population of the hydrogen excited states $n = 2$ and $n = 3$ was found less than 0.5% relative to the ground state at the electron density of $10^{12}\,\mathrm{cm}^{-3}$.
- Electron collisions with H_2, H_2^+ and H_3^+ (Table 1, 4-12): For electron collisions with the hydrogen molecule (reaction 5, 6 and 8) effective rate coefficient calculations were effectuated based on the Yacora model [17]. The RC model for molecular hydrogen includes the ground state and electronically excited states up to the principal quantum number $n = 10$. The individual electronic states are resolved up to $n = 3$ (e.g. $\mathrm{d}^3\Pi_\mathrm{u}$). For $n > 3$ this is not the case. The ground state, all states in $n = 2$ and the states $GK^1\Sigma_g^+$, $I^1\Pi_g$, $e^3\Sigma_u^+$ and $d^3\Pi_u$ in $n = 3$ are vibrationally resolved. Additional reactions and their reaction rates are selected from [21].
- Electron collisions with He, He^+ and He^{2+} (Table 1, 13-16): The effective reaction rates were obtained from the collisional radiative model NOMAD [18], using the recommended set of atomic data [22]. For He atoms the singlet and triplet states up to $n = 4$ (19 states) are considered independently and for He^+ ions the calculations are extended up to the first $n = 6$ excited states. Electron energy loss for collisions with He, He^+ and He^{2+}, including excitation, ionization and recombination, are implemented as cooling rates and are approximately independent on the electron density. The cooling rates are implemented in the electron energy balance equation

Table 1: Summary of the included elementary inelastic processes in hydrogen-helium plasmas.

		Reaction	Reference
		Electron collisions with H, H^+	
1.)	Excitation	$e + H \longrightarrow e + H^*$	see text
2.)	Ionization	$e + H \longrightarrow e + H^+ + e$	see text
3.)	Recombination	$e + H^+ \longrightarrow H + h\nu$	see text
		Electron collisions with H_2, H_2^+ and H_3^+	
4.)	Excitation	$e + H_2 \longrightarrow e + H_2^*$	[21]
5.)	Dissociation	$e + H_2 \longrightarrow e + H + H$	see text
6.)	Ionization	$e + H_2 \longrightarrow e + H_2^+ + e$	see text
7.)	Dissociative ionization	$e + H_2 \longrightarrow e + H^+ + H + e$	[21]
8.)	Recombination	$e + H_2^+ \longrightarrow H_2 + h\nu$	see text
9.)	Dissociation	$e + H_2^+ \longrightarrow e + H^+ + H$	[21]
10.)	Dissociative recombination	$e + H_2^+ \longrightarrow H + H$	[21]
11.)	Dissociative recombination	$e + H_3^+ \longrightarrow H + H + H$	[21]
		$e + H_3^+ \longrightarrow H_2 + H$	[21]
12.)	Dissociation	$e + H_3^+ \longrightarrow e + H^+ + H + H$	[21]
		Electron collisions with He, He^+ and He^{2+}	
13.)	Ionization	$e + He \longrightarrow e + He^+ + e$	see text
14.)	Recombination	$e + He^+ \longrightarrow He + h\nu$	see text
15.)	Ionization	$e + He^+ \longrightarrow e + He^{2+} + e$	see text
16.)	Recombination	$e + He^{2+} \longrightarrow He^+ + h\nu$	see text
		Ion impact reactions	
17.)	Charge exchange	$H^+ + H \longrightarrow H + H^+$	[24]
18.)	Charge exchange	$H^+ + H_2 \longrightarrow H + H_2^+$	[21]
19.)	Charge exchange	$H_2^+ + H_2 \longrightarrow H_2 + H_2^+$	[21]
20.)	Charge exchange	$He^+ + H \longrightarrow He + H^+$	[24]
21.)	Charge exchange	$He^+ + He \longrightarrow He + He^+$	[21]
22.)	Charge exchange	$He^{2+} + H \longrightarrow He^+ + H^+$	[25]
23.)	Charge exchange	$He^{2+} + He \longrightarrow He^+ + He^+$	[26]
24.)	Charge exchange	$He^{2+} + He \longrightarrow He + He^{2+}$	[21]
25.)	Formation of H_3^+	$H_2^+ + H_2 \longrightarrow H_3^+ + H$	[21]
26.)	Excitation	$H^+ + H \longrightarrow H^+ + H^*$	[21]
27.)	Excitation	$H^+ + H_2 \longrightarrow H^+ + H_2^*$	[21]
28.)	Ionization	$H^+ + H \longrightarrow H^+ + H^+ + e$	[21]
29.)	Ionization	$H^+ + He \longrightarrow H^+ + He^+ + e$	[21]
30.)	Dissociative ionization	$He^+ + H_2 \longrightarrow He + H^+ + H$	[21]

as

$$\dot{E}_e = ... - \Delta E^e_{\mathrm{He}}\, n_e\, n_{\mathrm{He}} - \Delta E^e_{\mathrm{He}^+}\, n_e\, n_{\mathrm{He}^+} - \Delta E^e_{\mathrm{He}^{2+}}\, n_e\, n_{\mathrm{He}^{2+}}. \quad (3)$$

Recombination reaction (14) includes both radiative recombination and dielectric recombination.

2.2.2. Inelastic ion impact reactions The included ion impact reactions are listed in Table 1 (17-30). The employed general formula to determine the reaction rate in

(Maxwellian) particle collisions from the cross section is given by

$$k(T_1, T_2) = \sqrt{\frac{2}{\pi}}\Big(\frac{m^*}{k_\mathrm{B}T^*}\Big)^{3/2} \int_0^\infty u^3 \sigma(u) e^{-\frac{m^* u^2}{2k_\mathrm{B}T^*}} \mathrm{d}u \tag{4}$$

with T_1 and T_2 the Maxwellian temperatures of the interacting particles, $T^* = (T_1 m_2 + T_2 m_1)/(m_1 + m_2)$ and $m^* = m_1 m_2/(m_1 + m_2)$ their reduced energy and mass, with m_1 and m_2 the masses of the interacting particles, k_B is the Boltzmann constant, $u = |\overrightarrow{v_1} - \overrightarrow{v_2}|$ is the impact velocity and $\sigma(u)$ the velocity dependent cross section [23]. The charge exchange reactions that have no effect on particle balances (reactions 17, 24, 21 and 24) are included since they are important for temperature equalization between ions and atoms or molecules. Reactions (28) and (29) are negligible for reduced temperatures below 100 eV.

2.2.3. Elastic processes Elastic collisions have a direct effect on the energy balance of the involved particles. Indirectly also the particle densities will be affected due to the energy dependent reaction rate coefficients. Since we require the model to predict the temperature and density of the plasma species in a self consistent manner, both the elastic Coulomb collisions between the charged particles and elastic ion-neutral and neutral-neutral collisions are included.

Energy transfers through Coulomb collisions between the charged particles are based on [27]. The resulting averaged energy transfer Q_c^{12} from population 1 to 2 is proportional to the difference of the Maxwellian temperatures of the two groups and the Coulomb collision frequency ν_{12}. It is implemented into the energy balance as:

$$\dot{E}_1 = ... - Q_c^{12} = ... - 3/2(T_1 - T_2)\nu_{12} n_1 \tag{5}$$

with n_1 and T_1 the particle density and temperature of the first group.

The relevance of elastic ion-neutral and neutral-neutral collisions was already shown for fusion edge plasmas for temperatures below 10 eV [28, 29, 30], and can be illustrated by comparing elastic collisions with their mutually related charge exchange collisions. The relation between the cross section for momentum transfer via elastic collisions σ_mt and charge exchange reactions σ_cx in homonuclear systems for the low energy region is approximately given by $\sigma_\mathrm{mt} = 2.21\sigma_\mathrm{cx}$ [31]. The reaction rates for elastic collisions are obtained via eq. (4), using momentum transfer cross sections from [32, 33, 34], and implemented in the model according to eq. (5).

2.3. Particle residence times and edge conditions

The confinement time of a particle can be expressed as a function of the dimensions of the vessel and the particle velocity towards the vessel walls. This velocity will depend on the considered physical mechanism. For losses of neutral particles the thermal velocity can be used. For charged particle losses one should consider separately the drift velocities, the diffusion velocity across the magnetic field and the ion velocity along the magnetic field lines.

2.3.1. Neutral wall fluxes To estimate the flux of neutrals (H, H_2, He) striking the walls, their mean free path, thermal velocity and the approximate average distance they need to travel to reach the walls of the toroidal chamber, are required. For the latter we take an approximate distance of two times the minor radius a, accounting for the fact that for all lines of sight that have a toroidal component, the average distance is larger that a. The mean free path λ_p of neutral particle 'p' is defined as

$$\lambda_p = v_{T,p} / \sum_{j,i} k^i_{jp}\, n_j \tag{6}$$

where $v_{T,p}$ is the thermal velocity of neutral p and the sum goes over the different species j in the plasma and over the possible reactions i between neutral p and particle j. The wall flux, or neutral particle loss term, is then estimated by defining their effective confinement time

$$\tau_p = \frac{2a}{v_{T,p}} e^{2a/\lambda_p} \tag{7}$$

which is in the 0D approach weighted by the probability that the particles will travel a distance of $2a$ without undergoing a collision (e^{-2a/λ_n}).

2.3.2. Ion wall fluxes The ion wall fluxes are constrained by the magnetic field. The axisymmetric magnetic configuration considered in the model consists of a high toroidal magnetic field B_θ (with $\vec{1}_\theta$ the toroidal direction), inhomogeneous in the radial direction ($\vec{1}_r$), to which a smaller homogeneous vertical field (B_z, with $\vec{1}_z$ the vertical upwards direction) is superimposed:

$$\vec{B}(r,z) = B_\theta(r_0)\frac{r_0}{r}\vec{1}_\theta + B_z\vec{1}_z \tag{8}$$

with r the radial position with respect to the torus center, r_0 the major radius of the toroidal axis and $B_\theta(r_0)$ the toroidal magnetic field strength on the toroidal axis.

Plasma drifts: It is known in controlled magnetic nuclear fusion that plasmas in this magnetic configuration are not in equilibrium. In the vertical direction the plasma is subject to '$\vec{B} \times \nabla B$' drifts stemming from the field curvature and gradient. The drift velocities are equal in size but in opposite direction for electrons and for ions, up for electrons and down for ions (for standard clockwise B_θ-direction). Charge cumulation in the plasma edge due to the '$\vec{B} \times \nabla B$' current induces a vertical electric field in the vessel, causing an outward drift velocity. Particle losses due to both drifts are included in the model. The vertical electric field is calculated self consistently from the vertical '$\vec{B} \times \nabla B$' current, the estimated short-circuit currents in the conductive vessel walls and the short-circuit currents running in the plasma along the magnetic field lines in case of an applied vertical magnetic field. For partially ionized plasmas ($T_e < 10\,\mathrm{eV}$) the radial drift is found to be negligible. The confinement time due to vertical drifts is inversely proportional to the particle energy, and of the order of 0.3 s for a 3 eV proton (for TEXTOR vacuum vessel dimensions and $B_\theta = 2.3\,\mathrm{T}$).

Losses along magnetic field lines: On application of a vertical magnetic field, the magnetic field lines will describe a spiral around the vertical torus axis, connecting

the bottom and top of the vessel. The connection length L from top to bottom depends on the magnetic fields and plasma radius a: $L\sin(\phi) = a$, with $\tan(\phi) = B_z/B_\theta$. When the connection length is of the order of the mean free path λ_p of the ions, losses along the magnetic field lines are significant. The vertical component of the velocity of a thermal ion is estimated as $v_{\mathrm{T},p}B_z/B_\theta$, with $v_{\mathrm{T},p}$ the thermal velocity.

Diffusion across the magnetic field: Charged particles diffuse across the toroidal magnetic field due to random collisions in the plasma. The diffusion coefficient is given by $D_\perp = \rho^2\nu_c$, with ρ the average step length the particle takes in collisions, and ν_c its collision frequency. The step length can be considered to be the gyration radius. In the well known Bohm scaling [35] the collision frequency is set equal to the cyclotron frequency, which results in a diffusion coefficient that only depends on the particle energy, and is valid for all charged plasma particles:

$$D_{\mathrm{Bohm}} = \frac{1}{16}\frac{k_b T}{eB} \tag{9}$$

where 1/16 is an empirical factor introduced by Bohm. The related diffusion velocity is [14]

$$v_{\mathrm{Bohm}} = \frac{2D_{\mathrm{Bohm}}}{a}. \tag{10}$$

The cross field diffusion coefficient has been estimated on TEXTOR via the radial plasma density decay length λ_d close to the wall. The latter was determined by two double Langmuir probes inserted in the plasma, resp. at the top and bottom of the vessel via the TEXTOR limiter locks, biased at $-100\,\mathrm{V}$. The toroidal magnetic field lines at these positions are limited by poloidal limiters, one at the top and one at the bottom of the vessel, so that the connection length L of the magnetic field lines equals one toroidal rotation $L = 11\,\mathrm{m}$. Fig. 1 shows the measured densities as function of the radial position on the left axis, cross checked with the total collected bias current on the structures (right axis) which is proportional to the plasma density. The observed background current and density values at large radial positions $|z| > 54\,\mathrm{cm}$ on the limiter lock 1 data are attributed to rectified RF current due to the proximity of the employed A2 RF antenna. The four data sets can be approximately fitted with a same exponential decay length of $\lambda_\mathrm{d} = 1.1\,\mathrm{cm}$ (dashed lines). For the typical modeled electron temperatures ($T_e \approx 3\,\mathrm{eV}$) the measured diffusion coefficient can be found from [36]

$$D_{\mathrm{meas}} = \frac{\lambda_\mathrm{d}^2 c_s}{L} \tag{11}$$

with c_s the ion sound velocity, which results in $D_{\mathrm{meas}} = 0.22\,\mathrm{m}^2/\mathrm{s}$. For the same electron temperature, and the applied toroidal magnetic field strength ($B_\theta = 2.3\,\mathrm{T}$) one obtains a Bohm diffusion coefficient of $D_{\mathrm{Bohm}} = 0.08\,\mathrm{m}^2/\mathrm{s}$, which is of the same order as the measured one, confirming Bohm diffusion in ICWC plasmas. For the above values the confinement time related to Bohm diffusion is of the order of $0.5 - 1.5\,\mathrm{s}$ (for TEXTOR vacuum vessel dimensions and $B_\theta = 2.3\,\mathrm{T}$).

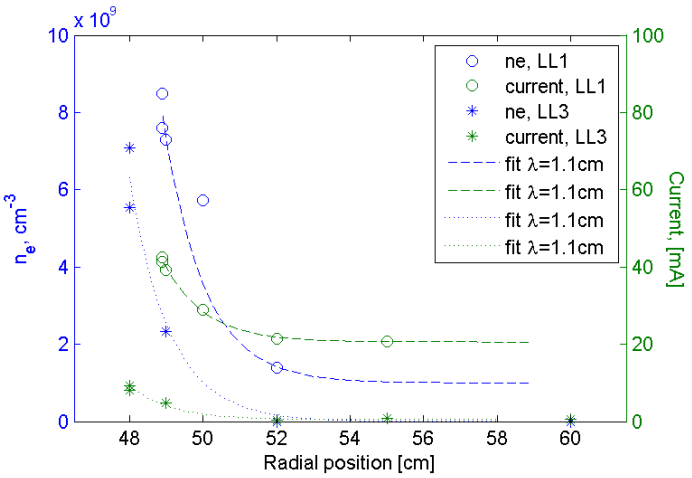

Figure 1: Measured decrease of electron density near vessel wall at bottom (LL1) and top (LL3) of the TEXTOR vessel, where the toroidal magnetic field lines are limited by poloidal limiters. Left axis: electron density by double Langmuir probe, right axis: collected current on biased probe holder ($-100\,\mathrm{V}$).

The above charged particle loss mechanisms are summarized in the following general formula for the ion confinement time:

$$\tau_p = \frac{a}{(v_{\mathrm{D}z,p} + v_{\mathrm{D}r,p} + v_{\mathrm{Bohm},p})e^{-a/\lambda_p} + v_{\mathrm{T},p}B_z/B_\theta e^{-aB_\theta/B_z\lambda_p}} \tag{12}$$

where λ_p the mean free path of the ion, $v_{\mathrm{D}z,p}$ is the '$\vec{B} \times \nabla B$' drift velocity, $v_{\mathrm{D}r,p}$ is the radial outward '$\vec{E} \times \vec{B}$' drift velocity, $v_{\mathrm{Bohm},p}$ is the cross field diffusion velocity and $v_{\mathrm{T},p}$ the thermal velocity of the ions. Eq. (12) estimating the particle confinement time is valid only for the plasma 'center' were the magnetic field lines are either closed or very long. The confinement time in the plasma 'edge' where the magnetic field lines are limited on in-vessel structures is much smaller due to losses along the magnetic field lines.

Fig. 2 shows the modeled influence of the ion confinement time on TEXTOR plasma parameters. The electron temperature and density, and the H^+-ion and H-atom density are plotted as a function of the confinement time, for a H_2-RF discharge with $p_{H_2} = 5{\cdot}10^{-4}\,\mathrm{mbar}$ and $P_{\mathrm{RF}} = 100\,\mathrm{kW}$. It is found that ion confinement times above $0.1\,\mathrm{s}$ have a minor influence on the plasma parameters. For smaller confinement times, the electron density will start to decrease leading, in this example, to a three times lower electron density in case of $\tau_p = 1\,\mathrm{ms}$, while the electron temperature increases. The above found values for vertical ion drifts and Bohm diffusion make that for partially ionized plasmas, the ion confinement time has only a minor influence on the plasma parameters.

In the model the electron losses are set to account for charge neutrality in the plasma. It is sometimes argued that electrons lose their energy faster than ions. To account for this one should include an energy confinement time that is smaller than the particle confinement time: $\tau_{p,e} \approx \chi\tau_{E,e}$, with $\chi > 1$. In the model we use $\chi = 3$ based

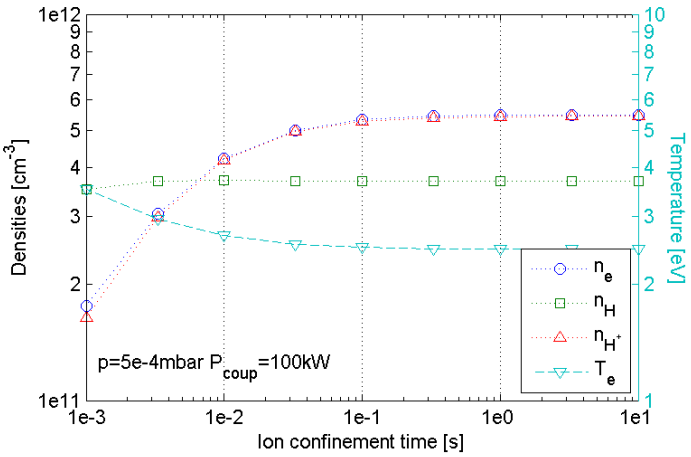

Figure 2: Modeled influence of the ion confinement time on plasma parameters for a partially ionized TEXTOR H_2-RF discharge with $p_{H_2} = 5 \cdot 10^{-4}$ mbar and $P_{RF} = 100$ kW. Above confinement times of 0.01 s the influence on the plasma density is minor. Typical confinement times are ~ 0.1 s for 3 eV ions.

on [12, 37, 38]. When the neutral gas is partially ionized, e.g. 20%, a change of χ from 1 to 3 decreases the plasma density only by 0.5%.

2.3.3. Edge conditions Neutrals, not affected by the magnetic field will be in constant interaction with the vessel walls. Also charged particles, due to their collective drifts, diffusion across the magnetic field, and transport along the field lines will interact with the walls. To describe the wall interaction in the model, the exchange of particles between wall and plasma is represented by the recycling coefficient R. From analysis of TEXTOR and TORE SUPRA mass spectroscopy data it is found that particle recycling in ICWC plasmas can be up to $R \geq 0.99$ [39]. The recycling in the model is assumed to be immediate. To properly add particle recycling in the balance equations, the main plasma wall interaction mechanisms have been considered. In the balance equations for neutral He and H_2 ($T_{He}, T_{H_2} < 10$ eV), the particle and energy reflection coefficient are set equal to 1, in close agreement with [40, 41]. Hydrogen atoms and ions in interaction with the wall either pick up a bounded H atom on the wall surface to form directly H_2 [42], or either penetrate into the wall to be desorbed later as H_2. Also the helium ions are neutralized by the wall and released with an energy equal to the wall temperature. The ions H_2^+ and H_3^+, having generally very low densities, are recycled as H_2. The implemented edge conditions appear as source terms in particle ($Q_{S,p}$, eq. (1)) and energy ($Q_{SE,p}$, eq. (2)) balance. A completer treatment of the wall interaction by coupling the 0D-model to a basic wall interaction module is presented in [43].

2.4. Discharge control parameters

The RF discharge control parameters are the discharge pressure, the gas mixture, the RF power and the magnetic field configuration. Below we discuss the implementation

of gas injection, active pumping, and the coupling of power into the balance equations.

2.4.1. Gas injection and active pumping In the 0D model, gas injection can be either regulated to keep the total pressure in the vessel constant (feedback controlled), or is pre-programmed at a given rate (feed forward). Terms for the removal rate of particles by the pumps and the injection rate appear in the particle balance as ($Q_{\mathrm{S},p}$ and $Q_{\mathrm{L},p}$ in eq. (1))

$$\dot{n}_{\mathrm{H}_2} = ... + Q_{\mathrm{H}_2,\mathrm{valve}} - n_{\mathrm{H}_2}\, S_{\mathrm{H}_2}/V_{\mathrm{pl}} \tag{13}$$

$$\dot{n}_{\mathrm{He}} = ... + Q_{\mathrm{He},\mathrm{valve}} - n_{\mathrm{He}}\, S_{\mathrm{He}}/V_{\mathrm{pl}} \tag{14}$$

with Q_{valve} the gas injection rate [$\mathrm{cm^{-3}s^{-1}}$], S the pumping speed [$\mathrm{cm^3s^{-1}}$] and V_{pl} the vessel volume [$\mathrm{cm^3}$]. The same terms come back in the energy balance, included in $Q_{\mathrm{S}E,p}$ and $Q_{\mathrm{L}E,p}$ in eq. (2).

2.4.2. Coupled power TOMCAT simulations show that the RF power coupled from the ICRF antenna to the RF plasma is absorbed mainly collisionally by electrons (typically $x \approx 75 - 90\%$) [44]. The remaining fraction $(1 - x)$ is coupled to the ions (all) by collisional absorption and to IC resonant ions by cyclotron absorption. The coupled RF power P_{RF} is included in the energy balance equation of the electrons ($xP_{\mathrm{RF}}/V_{\mathrm{pl}}$) and protons ($(1-x)P_{\mathrm{RF}}/V_{\mathrm{pl}}$). In the present 0D model however, only collisional absorption is considered, the population of resonant ions ($\sim 10^{-4} n_e$), determined from JET NPA measurements [5], modeled neutral densities and the charge exchange reaction rate (reaction 17, Table 1), being negligible.

Fig. 3 shows modeled plasma densities and Maxwellian energies for a TORE SUPRA hydrogen ICWC plasma, $p_{\mathrm{H}_2} = 5 \cdot 10^{-4}\,\mathrm{mbar}$ and $P_{\mathrm{RF}} = 100\,\mathrm{kW}$. The figure shows clearly that the electron density decreases when the fraction of coupled power to the electron decreases. This can be understood from the fact that electron impact ionization reactions are much more efficient than ionization on proton impact. Likewise the generally lower collisionality of the ions allow them to reach Maxwellian temperatures higher than 10 eV on increasing coupled power fraction ($1 - x > 0.5$). Higher ion energies might increase the wall conditioning efficiency of RF discharges. In the present understanding of ICWC discharges it is stated that most of the ICRF power is coupled to the electrons. In further modeling results we assumed $x = 1$.

2.5. Plasma impurities

Impurities in wall conditioning plasmas, either liberated by plasma wall interactions or from background neutral pressure in the vacuum vessel, strongly affect the plasma parameters. Fig. 4 shows electron cooling rates on neutral hydrogen, helium, carbon and oxygen, for a plasma with an electron density of $n_e = 10^{11}\,\mathrm{cm^{-3}}$, illustrating the importance of impurities. To obtain the actual energy loss per unit density one has to multiply with the density of the involved atom. The electron cooling rate on carbon

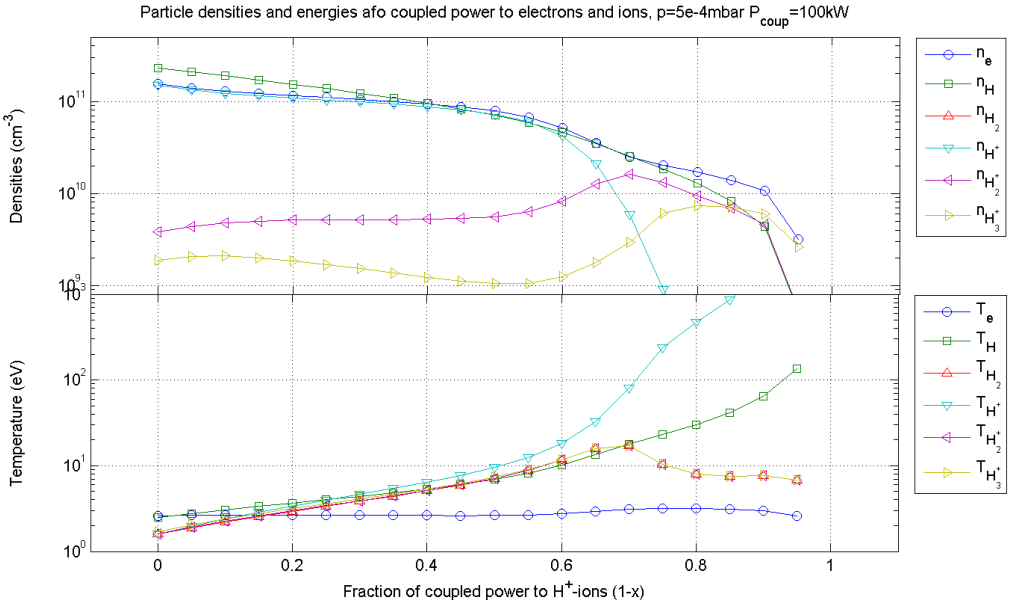

Figure 3: Modeled plasma densities (top) and Maxwellian energies (bottom) for a TORE SUPRA hydrogen ICWC plasma, $p_{\mathrm{H_2}} = 5 \cdot 10^{-4}\,\mathrm{mbar}$, $B_\theta = 3.8\,\mathrm{T}$ and $P_{\mathrm{RF}} = 100\,\mathrm{kW}$. The electron density decreases when the fraction of coupled power to the electron decreases while the ion temperature increases.

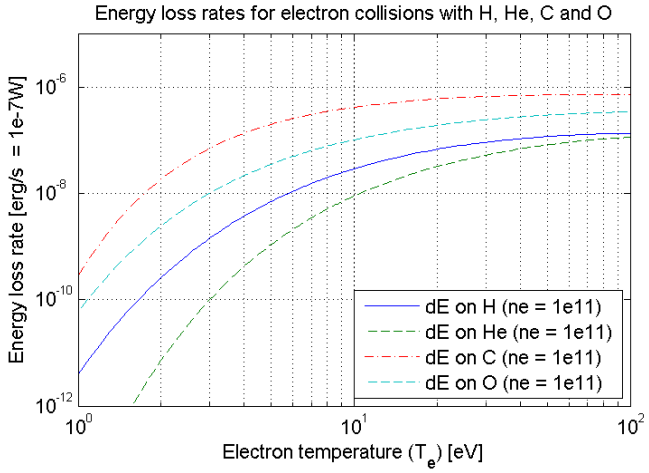

Figure 4: Total electron cooling rate for electron collisions with H, He, C and O as a function of the electron temperature, T_e ([45] = [INDC1995])

is two orders of magnitude higher than that of hydrogen, and almost three orders of magnitude than that of helium. The contributions of hydrogen and carbon to the total electron cooling in a low temperature hydrogen plasma (<10 eV) with 1% carbon impurities are thus of the same order of magnitude. In conditioning plasmas on machines with carbon facing components one expects mainly hydrocarbons, carbonoxides, and water as impurities. A proper consideration of the plasma impurities requires including particle and energy balance equations, containing elementary collisions, elastic collisions,

particle residence times, edge conditions and pumping of neutral molecules, for all the relevant impurity species and their ions. To enable a qualitative analysis on the effect of impurities, the 0D-model includes three extra particle balance equations, one for atomic carbon C and two for its ionized states C^+ and C^{2+}. The energy balance for the carbon species is not included. The electron energy balance is completed with cooling rates including excitation, ionization and recombination of carbon atoms and ions (data obtained from [45]), in the same manner as was done for helium (eq. 3). Also electron-ion Coulomb collisions are included in the electron energy balance equation. The electron particle balance is completed with carbon ionization reactions, that contribute to the electron density (data obtained from [33]). The actual production rate for carbon ions is however estimated to be lower than the given atomic carbon ionization rate. In the initial plasma phase, carbon will not be present as atoms, but rather as molecules due to its chemical reactiveness. For this same reason the electron cooling rate is estimated to be higher due to the numerous molecular excitational states and to molecule dissociation energies. Finally, the impurity ion confinement time is set to a constant value in accordance with [14].

Modeling results confirm that even small amounts of impurities have a large influence on the final electron density. For example a carbon impurity content of 1% of the total hydrogen pressure in a TEXTOR discharge of $p_{H_2} = 5 \cdot 10^{-4}$ mbar and $P_{RF} = 100$ kW (Fig. 3, $x = 1$) decreases the final electron density at least by a factor 2. Impurity contents of 1% are easily obtainable on TEXTOR. Fig. 5 shows CO and CH_4 partial pressures for four subsequent H_2-ICWC discharges in TEXTOR with feedback hydrogen pressure of $p_{H_2} = 5 \cdot 10^{-4}$ mbar and $P_{RF} \sim 60$ kW. According to the mass spectrometry data, and in accordance to baratron pressure data, there is a background CO pressure of approximately 4% of the feedback pressure. During the RF discharge (discharge initiation at $t = 2$ s, discharge ending at $t = 7$ s), the CH_4 partial pressure increases to approximately 2% of the feedback pressure. To be able to reproduce RF plasma parameters the plasma impurity content has to be known and their elementary collisions have to be accurately described in the balance equations. Unfortunately it is often difficult to estimate the exact impurity content and even the elementary collision data of molecules such as H_2O, CH_4 and CO is scarce. Nevertheless in the next section on modeling results we will show that the 0D model with carbon impurities is able to reproduce, at least qualitatively, the experimental data.

3. Modeling results

3.1. Plasma characteristics as a function of electron temperature

In an equilibrium situation, the plasma parameters can be brought back to the electron temperature. In this section we will illustrate independently of the discharge pressure and coupled power, the ion fraction data for a pure hydrogen plasma, a pure helium plasma, and a 50/50 H_2/He plasma. The pure gas ion fractions will be compared to the

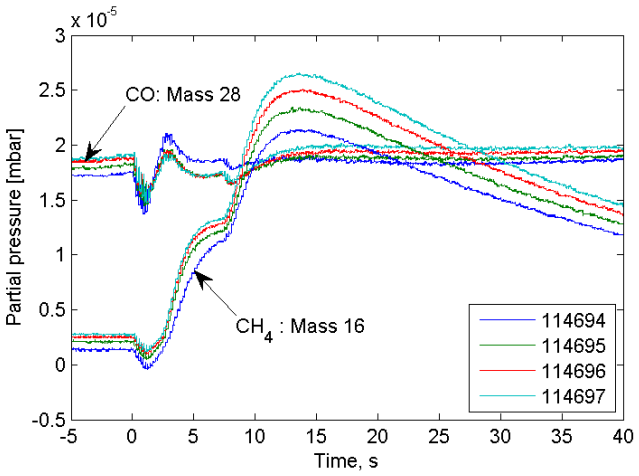

Figure 5: CO and CH_4 partial pressures from mass spectrometry for 4 subsequent H_2-ICWC discharges (discharge initiation at $t = 2\,\mathrm{s}$, discharge ending at $t = 7\,\mathrm{s}$) in TEXTOR with feedback hydrogen pressure of $p_{H_2} = 5 \cdot 10^{-4}\,\mathrm{mbar}$ and $P_{RF} \sim 60\,\mathrm{kW}$.

literature. In case of gas mixtures, there will be a clear influence of the mixture on the plasma parameters, especially in the temperature range where the plasma is partially ionized. The analysis is done for a perfectly confined plasma ($\tau_{ion} = 1000\,\mathrm{s}$).

3.1.1. Pure hydrogen plasma Fig. 6 (left, solid lines) gives the hydrogen ion fractions as a function of the electron temperature. To obtain sufficient ionization, the electron temperature needs to be above 2 eV. The transition from no ionization to full ionization happens completely in the electron temperature range of 2 to 2.8 eV. Steady state electron temperatures between these values can keep partially ionized plasmas. The presence of H_2^+ and H_3^+ is significant below 2.7 eV. In this example considering a perfectly confined plasma the H_3^+ density is almost equal to the electron density. In partially ionized plasmas the presence of H atoms is significant ($\sim 10\%$ of n_e). In fully ionized plasmas, the H atoms density is higher than that of the H_2 molecules, and both their concentrations decrease on increasing electron energy. The ratio of H ions and atoms is found to be in agreement with [46].

On taking into account the confinement properties of the plasma, the full ionization threshold temperature will shift to slightly higher values. Since ions and atoms are recycled as neutral molecules, the presence of neutrals at high temperatures will be more important in the case of the real ion confinement.

3.1.2. Pure helium plasma Fig. 6 (right, solid lines) gives the helium ion fractions as a function of the electron temperature. From electron temperatures of 2.2 eV on, the plasma attains a significant degree of ionization. The plasma is partially ionized in the electron temperature range from 2 to 3 eV. At $\approx 2.4\,\mathrm{eV}$ an ionization degree of 0.5 is obtained. A second transition, from the single ionized state to double ionized state, happens in the electron temperature range of 4 to 10 eV where, as the electron

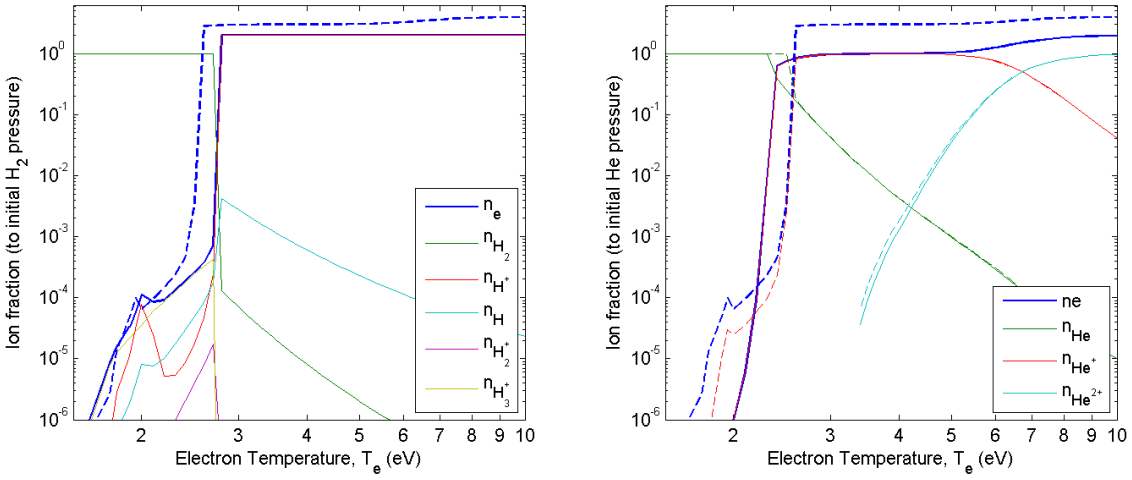

Figure 6: Ion fractions as a function of the electron temperature (T_e). Left: pure H_2 plasma (solid lines) and 50/50 He/H_2 plasma (dashed lines, only electron density). Right: Pure He plasma (solid lines) and 50/50 He/H_2 plasma (dashed lines).

temperature increases, the electron density increases likewise. A simultaneous presence of He and He^{2+} appears negligible (at $T_e = 4.2\,\text{eV}$ both are only $\approx 0.25\%$ of n_{He^+}). The modeled ion fractions are found to be in agreement with [46].

Similar as for the hydrogen case, by taking into account the confinement properties of the plasma, the full single ionization and double ionization threshold temperatures will shift to slightly higher values.

3.1.3. Hydrogen-helium mixtures On Fig. 6 also the electron density (resp. normalized to the initial hydrogen and helium density) and ion fractions (only for helium, right figure) for a neutral gas mixture of 50/50 H_2/He (dashed line) is plotted as a function of the electron temperature. The increased electron density in the temperature range of 2.1 to 2.5 eV due to ionized helium results in additional ionization of hydrogen. Consequently the full ionization state of hydrogen is reached somewhat earlier. The full ionization state of helium is reached somewhat later than for a pure helium plasma.

3.2. Plasma characteristics as a function of discharge pressure and coupled power

To benchmark the 0D model a comparison follows between model results, using experimental partial pressures and coupled RF power as model inputs, with experimental electron density data obtained from interferometry measurements. Once the density is modeled, additional information on the particle energies and main wall bombarding particle fluxes can be obtained. We will discuss TEXTOR H_2-ICWC discharge densities as function of RF power and pressure, TORE SUPRA He-ICWC discharge densities as function of RF power and TEXTOR H_2/He-ICWC discharge densities as function of the gas mixture.

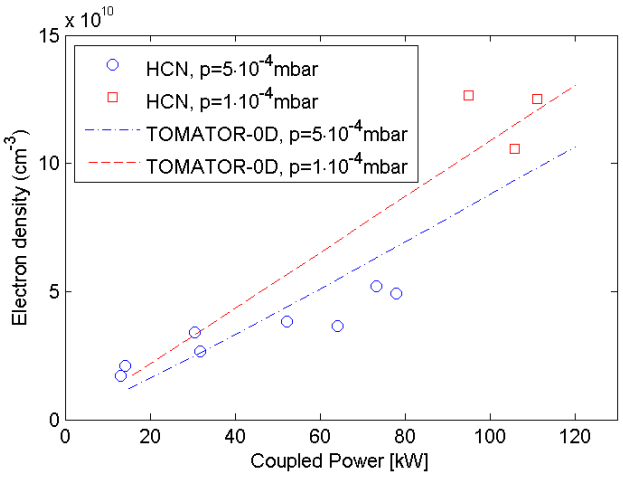

Figure 7: Modeled and experimental (HCN interferometry) TEXTOR ICRF plasma densities as a function of the coupled RF power to the electrons (feed back controlled pressures, $B_\theta = 2.3\,\mathrm{T}$, $B_z = 0.04\,\mathrm{T}$).

3.2.1. TEXTOR H_2-ICWC discharges Fig. 7 shows modeled and experimental TEXTOR ICRF plasma densities as a function of the coupled RF power to the electrons. The plots contain experimental data for RF discharges with a toroidal magnetic field of $B_\theta = 2.3\,\mathrm{T}$ and vertical field of $B_z = 0.04\,\mathrm{T}$. The pressure during these discharges was feedback controlled at $p_{\mathrm{H}_2} = 5 \cdot 10^{-4}\,\mathrm{mbar}$ or $p_{\mathrm{H}_2} = 1 \cdot 10^{-4}\,\mathrm{mbar}$. At a pressure of $p_{\mathrm{H}_2} = 5 \cdot 10^{-4}\,\mathrm{mbar}$ the measured electron density is of the order of $n_e = 4 \cdot 10^{10}\,\mathrm{cm}^{-3}$ ($P_{RF} = 50\,\mathrm{kW}$). For the same pressure and power, in absence of impurities, the 0D model predicts a ICWC plasma density of $n_e = 2.5 \cdot 10^{11}\,\mathrm{cm}^{-3}$. To match the experimental data the impurity content of the discharge was set to 1.5% for the high pressure case and consequently 7.5% for the five times lower feedback pressure case. These high impurity consentrations are realistic on TEXTOR, considering the evidenced high background CO pressure and increasing CH_4 pressure during the discharge (Fig. 5). The figure shows clearly that the density increases with increasing power. The modeled densities are in good agreement with the measurements.

Fig. 8 shows the modeled neutral and ion fluxes to the wall as a function of the coupled RF power, for both the high and low pressure cases. At high pressure the ion flux is negligible compared to the neutral atom flux, whereas at $p_{\mathrm{H}_2} = 1 \cdot 10^{-4}\,\mathrm{mbar}$, keeping the same impurity content, the neutral and ion wall flux becomes comparable. The neutral flux has decreased due to the smaller mean free path of the neutrals (higher electron density), and the lower neutral hydrogen pressure. The ions on the other hand will have a larger mean free path, due to their lower collisionality in the low pressure plasma, which significantly increases the number of particles reaching the vessel walls via transport along the magnetic field lines. The predicted temperature of these ions is in case of a partially ionized plasma around 2 to 3 eV. This temperature is not necessarily the impact energy on the wall since sheath effects can increase the energy significantly. The ion wall flux consist mainly of H^+. Both the neutral H and H^+ flux increase with

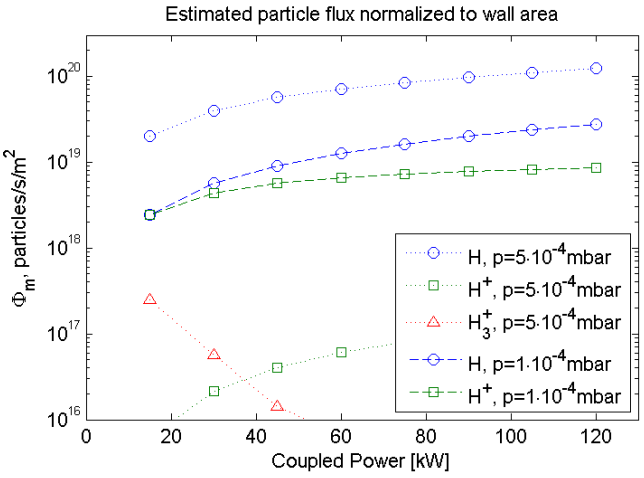

Figure 8: Modeled neutral and ion fluxes to the wall as a function of the coupled RF power, for the TEXTOR H_2-ICWC discharges given in Fig. 7.

the coupled RF power. The energy of the wall bombarding neutrals is about 3 eV, equal to the assigned average energy to the atoms on dissociation of hydrogen molecules. To obtain high ion fluxes to the wall one should aim at high RF powers, or low neutral gas pressures (high P_{RF}/N, with N the total amount of particles in the vessel).

The modeled neutral flux is in the range of the neutral flux that was predicted from partial H_2, HD and D_2 pressures, gas injection data and machine pumping speeds on TEXTOR, published in [39]. Also on TEXTOR the charged particle flux on a toroidal limiter blade, with a 0.5 m^2 surface, was measured. For a grounded toroidal limiter blade, the measured ion current was $9.3 \cdot 10^{17} \pm 1.3 \cdot 10^{17}$ /m^{2}s in case of hydrogen feedback pressure $p_{\mathrm{H_2}} = 5 \cdot 10^{-4}$ mbar and $16.5 \cdot 10^{17} \pm 0.5 \cdot 10^{17}$ /m^{2}s for $p_{\mathrm{H_2}} = 1 \cdot 10^{-4}$ mbar, both at a coupled RF power of $P_{\mathrm{RF}} \approx 100$ kW. The measured values are in the range of what is predicted by the 0D model, and the pressure dependence is qualitatively reproduced. The predicted ion flux in the low pressure case is however too high by a factor 4, and the predicted ion flux in the high pressure case is too low by a factor 8.

Finally the pumping probability $(1-f)$, with f the ionization probability, of neutral H_2 as a function of the electron density is shown on Fig. 9. The ionization probability is the probability that a neutral molecule will be ionized or dissociated instead of pumped out of the machine [14]. The evacuation of wall desorbed particles is very inefficient in a plasma with high ionization probability. From the figure it is clear that the pumping probability of H_2 for typical ICWC plasma densities of order $n_e \approx 10^{11}$ cm^{-3} is very low, in the range of 0.1%. Experimentally these low values are confirmed [39]. To optimize the conditioning efficiency it is clear that a compromise has to be sought between the high wall fluxes on one side (neutrals: high power, high pressure; ions: high power, low pressure) and the reionization probability on the other. An alternative solution is to operate the discharges in pulsed mode: ~ 1 s discharges followed by sufficient pumping time (order of a few times the characteristic pumping time) [39].

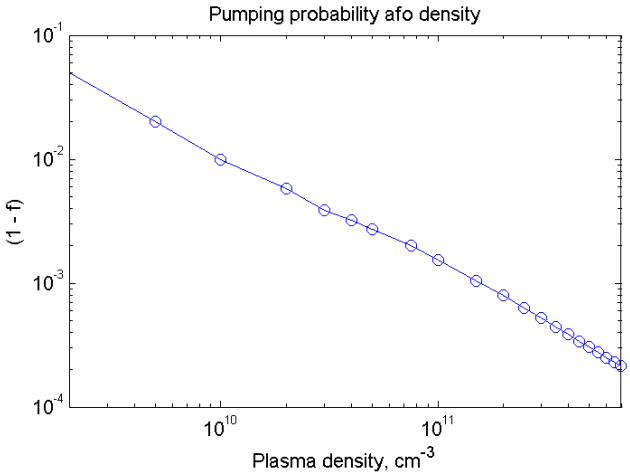

Figure 9: Pumping probability $(1-f)$ of neutral H_2 as a function of the electron density for TEXTOR discharges.

3.2.2. TORE SUPRA He-*ICWC discharges* Fig. 10 shows both experimental and modeled helium plasma densities as a function of the coupled power for TORE SUPRA He-ICWC discharges at pressure $p_{\mathrm{He}} = 1.8 \cdot 10^{-4}\,\mathrm{mbar}$, $B_\theta = 3.8\,\mathrm{T}$ and $B_z = 0\,\mathrm{T}$. The neutral hydrogen content during these discharges, released by the wall due to the plasma wall interaction, is set constant to $p_{\mathrm{H_2}} = 8 \cdot 10^{-6}\,\mathrm{mbar}$ in accordance with experimental partial pressures. To match the experimental data a reasonable impurity content of 0.35% is added to the neutral pressure (the impurity content during TORE SUPRA ICWC discharges is found to be much lower than on TEXTOR). A helium plasma

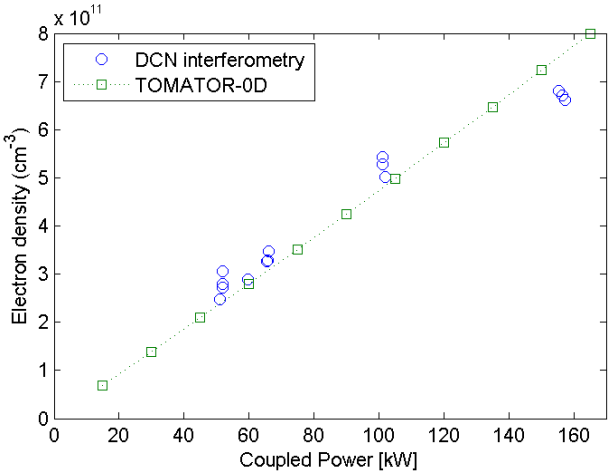

Figure 10: Experimental (DCN interferometry) and modeled helium plasma densities as a function of the coupled power for TORE SUPRA He-ICWC discharges at pressure $p_{\mathrm{He}} = 1.8 \cdot 10^{-4}\,\mathrm{mbar}$, $p_{\mathrm{H_2}} = 8 \cdot 10^{-6}\,\mathrm{mbar}$ (stemming from wall interaction), $B_\theta = 3.8\,\mathrm{T}$ and $B_z = 0\,\mathrm{T}$.

has generally a higher plasma density ($n_e \approx 4 \cdot 10^{11}\,\mathrm{cm}^{-3}$) than a hydrogen plasma ($n_e \approx 4 \cdot 10^{10}\,\mathrm{cm}^{-3}$) for the same coupled power at a given pressure. The density in

He-plasmas is linear with the coupled RF power. Fig. 11 shows the modeled particle fluxes to the wall as a function of the coupled RF power. As in case of a pure hydrogen plasma, the fluxes increase with power and with density. Interestingly it is found that the main wall bombarding species are neutral H-atoms. The He^+-ion flux is approximately equal to the H^+-ion flux. The 0D model reveals thus clearly that in case of helium wall conditioning discharges, the wall released hydrogen particles will largely contribute to the wall bombarding flux.

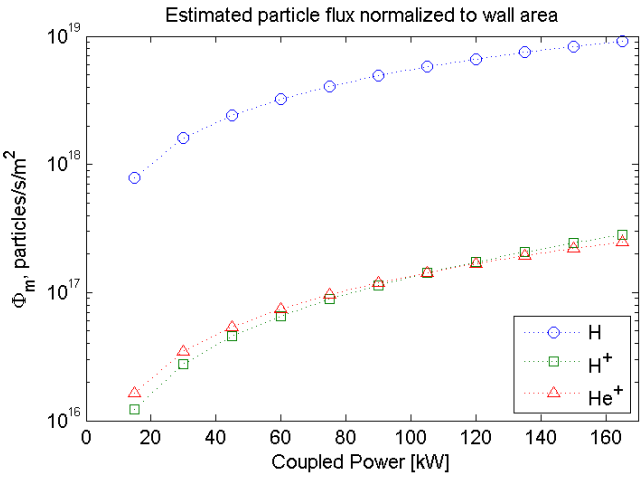

Figure 11: Modeled particle fluxes to the wall as a function of the coupled RF power, for the TORE SUPRA He-ICWC discharges given in Fig. 10.

3.2.3. TEXTOR H_2*/*He*-ICWC discharges* Fig. 12 shows the influence of the neutral gas mixture on the electron density for a series of TEXTOR discharges with constant helium injection and feedback hydrogen injection ($p_{\mathrm{tot}} = 5 \cdot 10^{-4}$ mbar). For a helium concentration concentration below 50% the electron density is as in previous examples lower than $10^{11}\,\mathrm{cm}^{-3}$ (interferometer density, blue rectangles). On higher helium concentrations the electron density increases abruptly to values around $3.5 - 5.5 \cdot 10^{11}\,\mathrm{cm}^{-3}$. On the right axis the coupled power during these discharges is given. Except for one single discharge with a helium concentration of 53%, the coupled power (green dots) in the discharges increases monotonically with the helium concentration, although the RF generator power was kept constant for all discharges, which means that the RF coupling efficiency increases with increasing helium concentration. From RF physics point of view one would expect that the coupling efficiency is firstly dependent on the electron density rather than on the gas mixture. Since the coupling efficiency doesn't show the same discontinuity as the plasma density, it is expected that the increase of density is due to collisional processes. On the figure also modeled densities are given (blue triangles). The densities are modeled by adjusting the input coupled power proportional to the gas mixture, according to the experimental coupled powers. The model input powers are given by the green rectangles. The hydrogen injection in the modeling is like in the experiment controlled to keep the total pressure constant,

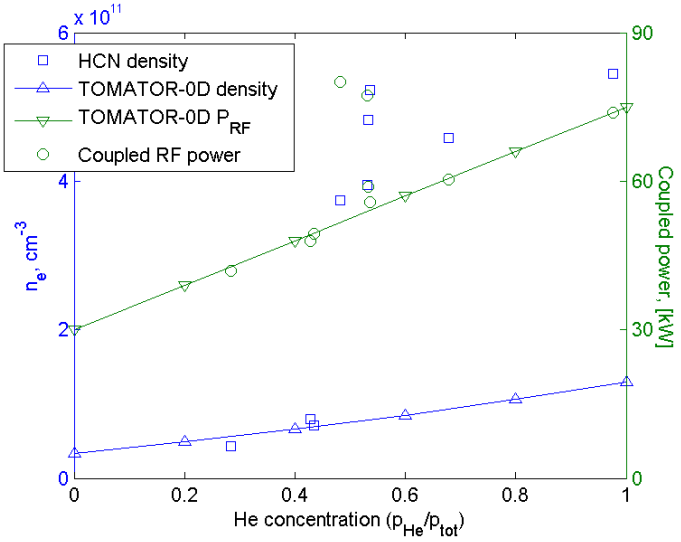

Figure 12: Influence of the neutral gas mixture on the electron density for a series of TEXTOR discharges with constant helium injection and feedback controlled hydrogen injection ($p_{\mathrm{tot}} = 5 \cdot 10^{-4}$ mbar). The RF coupling efficiency increases linearly with increasing helium concentration. The plasma density shows a discontinuous increase around He/H_2-concentrations $\approx 50/50$ which is presently not reproducible with the 0D model.

while the helium injection is kept continuously constant. In accordance with previous TEXTOR example, the impurity concentration is set to 1.5% of the total pressure. It is clear from the figure that the model is able to reproduce the density in case of a hydrogen like plasma (helium concentration lower than 50%). However it does not reproduce the sudden density increase observed on higher helium concentration. The imperfect description of plasma impurities in the model is thought to lie at the origin of this, but in this stage of the model also the influence of RF coupling properties can't be ruled out. It is therefore envisaged to upgrade the 0D model to include a RF power coupling module based on full wave code TOMCAT, which should preferentially be done in a 1D context.

Conclusion

In this paper the 0D description of magnetized toroidal hydrogen-helium RF discharge is presented. The model is developed to obtain insight on ICRF plasma parameters, particle fluxes to the walls and the main collisional processes, which is especially relevant for the comprehension of RF wall conditioning discharges, for which hydrogen and helium are the most common discharge gases. The 0D plasma description is based on the energy and particle balance equations for 9 principal species: H, H^+, H_2, H_2^+, H_3^+, He, He^+, He^{2+} and e^-. It takes into account (1) elementary atomic and molecular collision processes, such as excitation/radiation, ionization, dissociation, recombination, charge exchange, etc... and elastic collisions, (2) particle losses due to the finite dimensions of the plasma volume and confinement properties of the magnetic configuration, and

particle recycling, (3) active pumping and gas injection, (4) RF heating of electrons (and protons) and (5) a qualitative description of plasma impurities. The typically low temperature wall conditioning plasmas motivate the implementation of molecular hydrogen.

It is found that experimentally evidenced impurity concentrations have an important impact on plasma parameters. The effect of impurities on the plasma parameters is simulated by including balance equations for C, C^+ and C^{2+}. On inclusion of plasma impurities the model reproduces experimental plasma density dependencies on discharge pressure and coupled RF power, both for hydrogen RF discharges ($n_e \approx 1 - 5 \cdot 10^{10}\,\mathrm{cm}^{-3}$) as for helium discharges ($n_e \approx 1 - 5 \cdot 10^{11}\,\mathrm{cm}^{-3}$). The modeled wall fluxes of hydrogen discharges are in the range of what is estimated experimentally: $\sim 10^{19} - 10^{20}\,/\mathrm{m}^2\mathrm{s}$ for H-atoms, and $\sim 10^{17} - 10^{18}\,/\mathrm{m}^2\mathrm{s}$ for H^+-ions. In case of helium RF discharges it is found that wall desorbed hydrogen contributes largely to the wall flux. The main wall bombarding flux consists of hydrogen neutrals. The helium and hydrogen ion flux are approximately of the same order of magnitude although the hydrogen neutral pressure, stemming from wall desorption, is in accordance to mass spectrometry data less than 5% of the helium neutral pressure.

The sudden increase of plasma density on increasing the discharge helium concentration, while keeping the total pressure constant, as observed on TEXTOR could not be reproduced by the 0D model. Since the coupled power, and thus the coupling efficiency does not show a similar discontinuity, it is nevertheless expected that collisional processes lie at the basis of this effect. A future upgrade of the 0D model to 1D, including a self consistent description of the coupled RF power, and reconsideration of the inclusion of plasma impurities is required to evidence this.

Acknowledgments

This work was supported by EURATOM and carried out within the framework of the European Fusion Development Agreement. The views and opinions expressed herein do not necessarily reflect those of the European Commission. The authors would like to thank the TORE SUPRA and TEXTOR team for their excellent assistance and support of this work.

References

[1] A. Lyssoivan et al., J. Nucl. Mat. **337-339**, 456 (2005)
[2] D. S. Lee et al., Trans. Fus. Sci. Tech. **94-97**, 60 (2011)
[3] J. S. Hu et al., J. Nucl. Mater. **207-210**, 376 (2008)
[4] R. Brakel, D. Hartmann, and P. Grigull, J. Nucl. Mat. **290-293**, 1160 (2001)
[5] D. Douai et al., J. Nucl. Mat. *doi:10.1016/j.jnucmat.2010.11.083*, (2010).
[6] J. Roth et al., Plasma Phys. & Controlled Fusion **50**, 103001 (2008).
[7] M. Shimada and R. A. Pitts, J. Nucl. Mat. *doi:10.1016/j.jnucmat.2010.11.085*, (2010).
[8] R. Koch et al., in *26th EPS Conference on Controlled Fusion and Plasma Physics, Maastricht - 14/18 June*, volume 23J, page 745, 1999.

[9] V. Plyusnin et al., in *Proceedings of ISC-11 & ITC-8 - Helical System Research*, volume 1, 1998.
[10] A. Lyssoivan, *Probl. At. Sci. Tech.*, volume 1 of *Plasma Physics*, pages 30–34, 2007, issue $N^0$13.
[11] T. Wauters et al., *38th EPS Conference on Controlled Fusion and Plasma Physics, Strasbourg*, 2011
[12] A. Lyssoivan and et al., Nucl. Fusion **32**, 1361 (1992).
[13] V. E. Moiseenko et al., Fusion Eng. & Design **26**, 203 (1995).
[14] E. de la Cal, Plasma Phys. & Controlled Fusion **48**, 1455 (2006).
[15] B. Lloyd, P. G. Carolan, and C. D. Warrick, Plasma Phys. & Controlled Fusion **38**, 1627 (1996).
[16] S. I. Braginskii, Transport Processes in a Plasma, in *Reviews of Plasma Physics 1*, New York, 1965, Consultants Bureau.
[17] D. Wünderlich, S. Dietrich, and U. Fantz, J. Quant. Spectrosc. Radiat. Transfer **110**, 62 (2009).
[18] Y. V. Ralchenko and Y. Maron, J. Quant. Spectrosc. Radiat. Transfer **71**, 609 (2001).
[19] I. I. Sobelman, L. A. Vainshtein, and E. A. IUkov, *Excitation of atoms and broadening of spectral lines*, Springer-Verlag, Berlin, New York, 1981.
[20] I. Bray and Y. Ralchenko, CCC-database, http://atom.curtin.edu.au/CCC-WWW/.
[21] D. Reiter, The data file HYDHEL: Atomic and Molecular Data for EIRENE, Forschungszentrum Juelich GmbH, 52425 Juelich, 2002
[22] Y. Ralchenko et al., Atomic Data and Nuclear Data Tables **94**, 603 (2008).
[23] O. Marchuk et al., Journal of Physics B: Atomic, Molecular and Optical Physics **40**, 4403 (2007).
[24] V. Shevelko et al., One-electron Capture and Target Ionization in He+-neutral-atom Collisions, Technical report, NIFS, 2009.
[25] R. Janev and J. J. Smith, Atomic and Plasma-Material Data for Fusion, a supplement to J. Nucl. Fusion**4** (1993).
[26] M. B. Shah, P. McCallion, and H. B. Gilbody, J. Phys. B-At. Mol. Opt. **22**, 3037 (1989).
[27] D. V. Sivukhin, Coulomb Collisions in a Fully Ionized Plasma, in *Reviews of Plasma Physics 4*, New York, 1966, Consultants Bureau.
[28] H. H. Abou-Gabal and G. A. Emmert, Nucl. Fusion **31**, 407 (1991).
[29] D. Reiter, P. Bachmann, and A. K. Prinja, Contributions to Plasma Physics **32**, 261 (1992).
[30] P. Bachmann and D. Reiter, Contributions to Plasma Physics **35**, 45 (1995).
[31] R. K. Janev, Contributions to Plasma Physics **38**, 307 (1998).
[32] R. K. Janev, editor, *Atomic and Molecular Processes in Fusion Edge Plasmas*, 1995.
[33] D. Reiter, The data file AMJUEL: Additional Atomic and Molecular Data for EIRENE, Forschungszentrum Juelich GmbH, 52425 Juelich, 2010.
[34] A. V. Phelps, J. Phys. Chem. Ref. Data **19**, 653 (1990).
[35] J. Wesson, *Tokamaks*, Oxford Science Publications, Clarenden Press, Oxford, 2^{nh} edition, 1997.
[36] B. Unterberg, Trans. Fus. Sci. Tech. **57** (2010), Number 2T, FUSTE8 (2) 1-504.
[37] J. Buermans and T. Matthys, 0-D Transport Modeling of the RF Plasma Production in a Fusion Reactor, Master's thesis, Royal Military Academy (Brussels), 2006.
[38] A. Lyssoivan, Energy and particle balance equations for RF plasmas in fusion machines, Report, Royal Military Academy (Brussels), 2007.
[39] T. Wauters et al., J. Nucl. Mat. *doi:10.1016/j.jnucmat.2010.11.072* (2010).
[40] W. Eckstein, Calculated Sputtering, Reflection and Range Values, Technical report, Max Planck Society - eDocument Server, Germany, 2002.
[41] E. Vietzke, J. Nucl. Mat. **266**, 324 (1999).
[42] M. Rutigliano and M. Cacciatore, ChemPhysChem **9**, 171 (2008).
[43] D. Douai et al., AIP Conference Series, *19th Topical Conference on Radio Frequency Power in Plasmas, Newport*, 2011
[44] A. Lyssoivan et al., *38th EPS Conference on Controlled Fusion and Plasma Physics, Strasbourg*, 2011
[45] R. Marchand, C. Illescas, X. Bonnin, and J. Botero, Radiative Losses and Electron Cooling Rates of Hydrogen, Helium, Carbon and Oxygen, IAEA Nuclear Data Section, 1400 Vienna, Austria,

1995.
[46] M. Arnaud and R. Rohtenflug, Astronomy and Astrophysics Supplement Series **60**, 425 (1985).